Electronic Supplementary Material (ESI) for Soft Matter.

Closer insight in the structure of moderate to densely branched combs by combining modeling and linear rheological measurements

-Supporting Information-

1. Synthesis of combs

In this contribution, we use a grafting-from approach based on an ATRP mechanism to synthesize well-defined PnBA combs in which the length of the PnBA backbone, the number of grafted PnBA chains and the length of the PnBA grafts can be controlled by tuning the experimental conditions. The synthesis approach includes: (a) synthesis of backbone copolymer (b) cleavage of the protecting groups to provide multi-functional macro-initiator and (c) growth of side branches.

Conversions during the synthesis of backbone copolymers were followed by HNMR as shown in Figure SI1. The CH_2 unit in the pendant group exists in both monomers and polymer chain and appears at 4.16 ppm for BA and at 4.1 for HEA-TMS, while protons appeared at 5.8, 6.1 and 6.4 ppm only belong to monomers. These peaks weaken during the polymerization course which can be used for determination of monomer conversions

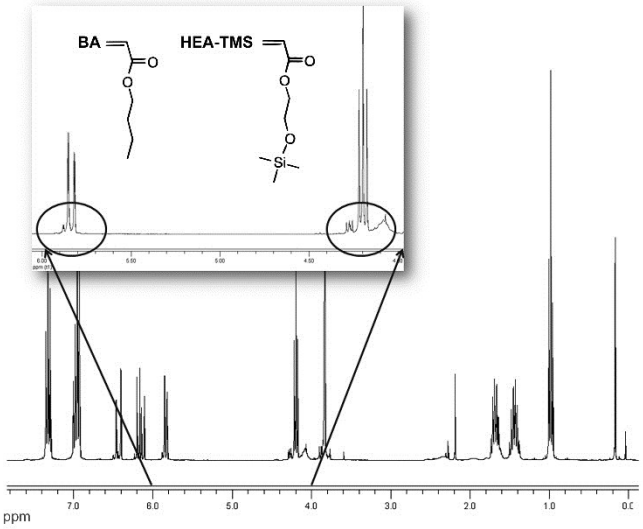

Figure SI1. HNMR spectrum of the reaction mixture during polymerization of linear chains.

Figure SI2 shows the ^{1}H NMR spectrum of the purified P(nBA-*co*-HEA). The presence of broad peaks between 3.9 and 4.2 ppm due to respectively, the O**CH$_2$** in nBA and HEA units (labeled a and e, respectively) and the methyl of the pendant in nBA units in 0.96 ppm (labeled d) and 0.13 ppm belonging to methyl of TMS groups in HEA units (labeled g), illustrates the presence of both comonomers in the P(nBA-*co*-HEA). The final copolymer compositions were determined by ^{1}H NMR spectroscopy. The integration area of O**CH$_2$** from nBA and HEA-TMS units (labeled a and e) and 9 protons of trimethylsiloxy group around 0.13 ppm (labeled g) from HEA units were compared to get final copolymer composition.

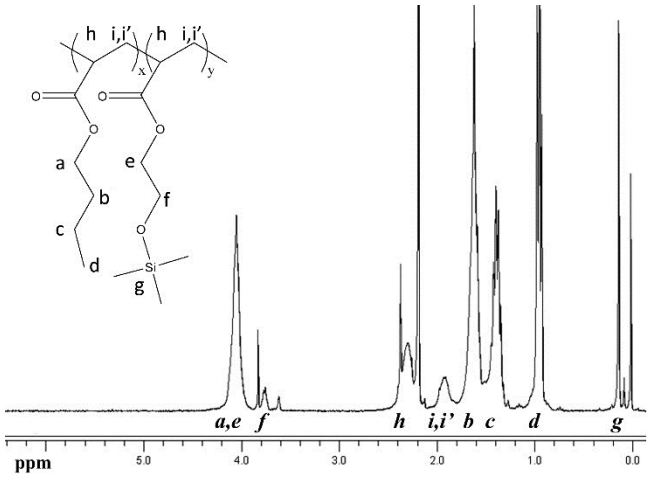

Figure SI2. ^{1}H NMR spectrum of purified P(nBA-*co*-HEA) (BB4).

Relative molar masses of the linear precursors and homopolymers were measured by SEC and Molecular Weight Distributions (MWDs) are shown in Figure SI3. All samples have similar symmetric distributions.

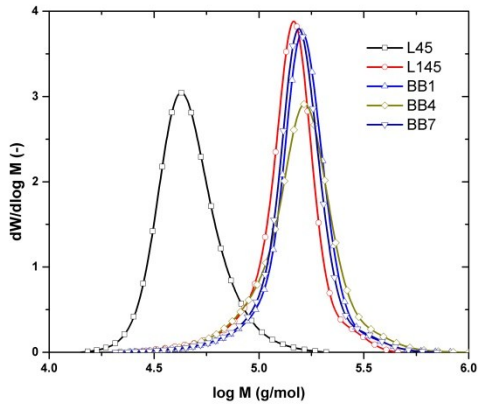

Figure SI3. Molar mass distribution of linear polymers.

Figure SI4 shows the ^{1}H NMR spectrum of the final comb structure. As expected the ^{1}H NMR spectrum of the comb is not different from the spectrum of the linear PnBA.

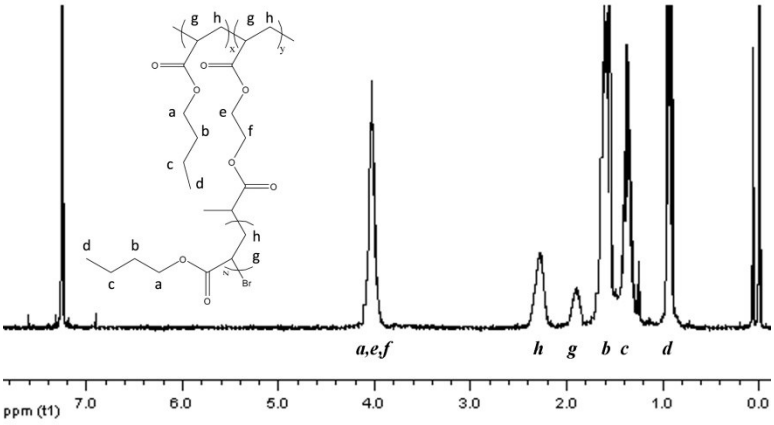

Figure SI4. ^{1}H NMR spectrum of PNBA-*g*-PNBA comb C4-4.

2. Deconvolution of MWDs

Deconvolution of MWD curves into several log normal distributions can be useful to study the variation of different parts of the peaks as conversion proceeds. Deconvoluted peaks are depicted in Figure SI5, SI6 and SI7, for comb series C1, C4 and C7, respectively. Normally three standard functions were needed to capture low molar mass shoulder, main peak and high molar mass coupled combs. However, for some samples, coupled combs were negligible and two functions were sufficient to capture the whole MWD peak. Results of the corresponding weight fractions, weight average molecular weight and polydispersity indices are summarized in Table SI1.

Table SI1. Deconvolution of MWD into three log normal distribution functions.

	Fraction #1			Fraction #2			Fraction #3		
	Wt.%	Mw (kg/mol)	D	Wt.%	Mw (kg/mol)	D	Wt.%	Mw (kg/mol)	D
C1-9	0.04	50	1.1	0.86	232	1.08	0.08	509	1.07
C1-21	0.13	109	1.2	0.71	351	1.14	0.14	700	1.12
C4-4	0.11	135	1.13	0.86	371	1.16			
C4-7	0.18	179	1.2	0.79	481	1.2			
C4-13	0.18	160	1.26	0.8	579	1.36	0.01	1856	1.04
C4-19	0.09	104	1.3	0.88	716	1.2	0.02	2430	1.07
C7-11	0.06	189	1.1	0.72	543	1.14	0.2	1418	1.13
C7-28	0.03	300	1.2	0.77	1382	1.5	0.2	2854	1.25

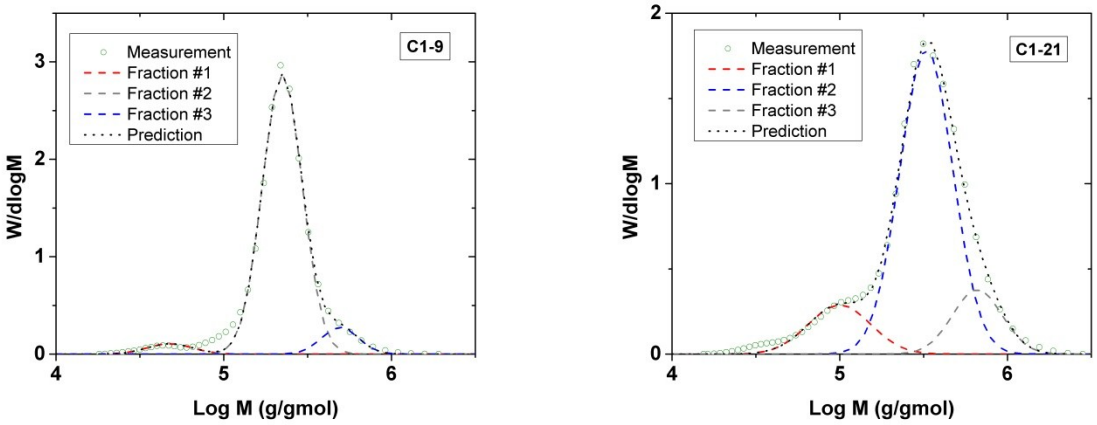

Figure SI5. Deconvolution of C1 comb series into standard functions.

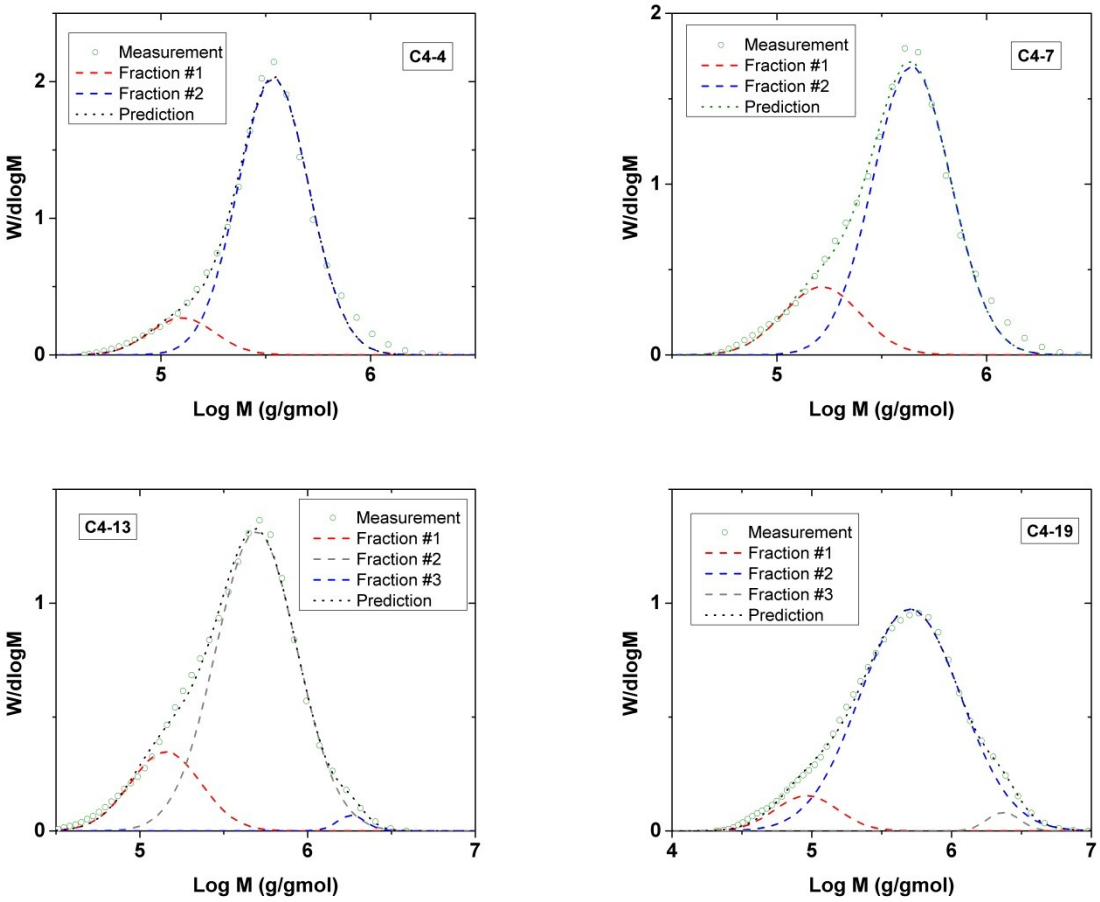

Figure SI6. Deconvolution of C4 comb series into standard functions.

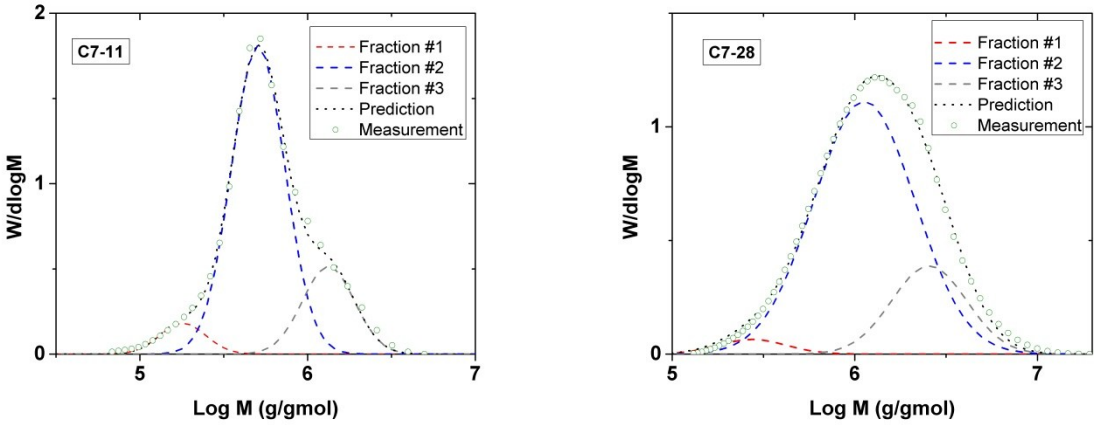

Figure SI7. Deconvolution of C7 comb series into standard functions.

3. Rheological properties of linear samples

Linear samples including the L145 and BB1, BB4 and BB7 backbones have very similar molar mass and distributions. Their linear rheological properties are therefore expected to be superimposable if the comonomer incorporation does not make any morphological or structural changes. The dynamic moduli of linear samples are compared in Figure SI8. The slight difference can be attributed to the variation in their molar mass.

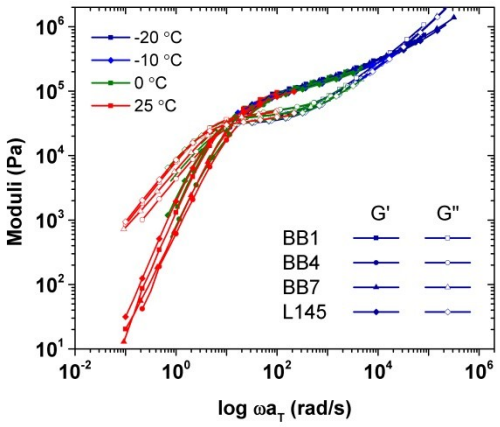

Figure SI8. Comparing the linear rheological properties of linear homo and copolymer backbones.

4. Rheological modeling

4.1. General algorithm

A simple rheological model was developed based on TMA to capture the rheological behavior in the intermediate frequency region. The comb structure was replaced by a binary blend of monodisperse chains representing branches and backbone. The branches could not reptate but were allowed to fluctuate from time zero while the backbone fraction had a very long relaxation time. All the mechanisms involved in the relaxation of polymers, i.e. high frequency Rouse relaxation, dynamic dilution and constraint release were also activated. The length and fraction of branches were adjusted to capture the dynamic moduli especially in the intermediate frequency zone.

4.2. TMA model

Details of TMA model for linear and star chains are already described elsewhere [1]. Brief descriptions of model components are given below. Symmetric stars can mainly relax by contour length fluctuations according to the following probability:

$$p_{fluc}(x,t) = exp\left(\frac{-t}{\tau_{fluc}(x)}\right) \quad \text{(S.1)}$$

The specific lifetime for fluctuations is determined by free Rouse motions for the segments near extremities, while deeper segments need to overcome the retraction's potential penalty:

$$\tau_{early}(x) = \frac{9\pi^3}{16}\tau_e x^4 Z^4 \quad \text{(S.2)}$$

$$\tau_{late}(x) = \tau_0 exp\left(\frac{U(x)}{kT}\right) \quad \text{(S.3)}$$

$$U(x) = \frac{3kT}{2Nb^2}(L_{eq}x)^2 + cons \quad \text{(S.4)}$$

Since the relaxation times of deep segments are exponentially separated, they can use the already relaxed part of the chain as solvent to dilate the confining tube according to dynamic dilution. It worth mentioning that in this specific case the backbone is considered to not relaxing. Transition between the early and late fluctuations modes happens at the segment where the potential barrier is equal to the systems thermal energy.

Linear chains can also reptate at the specific reptation lifetime according to the following probability:

$$p_{rept}(x,t) = \sum_{i,odd} \frac{4}{i\pi} sin\left(\frac{i\pi x}{2}\right) exp\left(\frac{-i^2 t}{\tau_{rept}}\right) \quad \text{(S.5)}$$

$$\tau_{rept} = 3\tau_e Z^3 \phi_{active}^{\alpha}(t) \quad \text{(S.6)}$$

where $\phi_{active}(t)$ is the fraction of already relaxed segments that reptation can use to dilate the confining tube based on the Graessley's criterion and $\alpha=1$ is the dilution exponent.

The fraction of oriented chains can be calculated at each time step, from the fraction of segments that are yet relaxed neither by reptation nor by fluctuations:

$$\phi(t) = \sum_i \varphi_i \int_0^1 (p_{rept}(x,t) p_{fluc}(x,t)) dx \quad \text{(S.7)}$$

where φ_i is the weight fraction of star and linear chain. As the neighboring chains can also relax, the confining tube also relaxes by constraint release process. The probability of tube relaxation is equal to the probability of chain relaxation, while it cannot be faster than what lateral Rouse movements may allow:

$$\phi_{CR}(t_i) \geq \phi_{CR}(t_{i-1})\left(\frac{t_{i-1}}{t_i}\right)^{0.5} \tag{S.8}$$

The transient modulus can be calculated by inclusion of high frequency fast modes and longitudinal slow modes of Rouse motion:

$$G(t)/G_N^0 = \phi(t)\phi_{CR}^{\alpha}(t) + F_{Rouse,long}(t) + F_{Rouse,fast}(t) \tag{S.9}$$

$$F_{Rouse,long}(t) = \sum_i \frac{\varphi_i}{4Z_i} \sum_{j=1}^{Z_{i-1}} exp\left(\frac{-j^2 t}{\tau_{Rouse,i}}\right) \tag{S.10}$$

$$F_{Rouse,fast}(t) = \sum_i \frac{5\varphi_i}{4Z_i} \sum_{j=Z_i}^{N} exp\left(\frac{-2j^2 t}{\tau_{Rouse,i}}\right) \tag{S.11}$$

where Z corresponds to the chain's span and the specific Rouse relaxation time is:

$$\tau_{Rouse} = \tau_e Z^2 \tag{S.12}$$

Schwarzl method was used to convert transient modulus to dynamic storage and loss moduli. The molar mass and fraction of star chains were adjusted using Nelder-Mead simplex method to capture the dynamic moduli measured by frequency sweep. The following error function was defined and minimized in the optimization course:

$$\chi = \frac{1}{n}\sum_{i=1}^{n}\left[\frac{(G_{exp}^{'}(i) - G_{the}^{'}(i))^2}{G_{exp}^{'}(i)^2} + \frac{(G_{exp}^{''}(i) - G_{the}^{''}(i))^2}{G_{exp}^{''}(i)^2}\right]$$

(S.13)

4.3. Model verification

Before the application of model for evaluation of the length of side branches in the synthesized samples, it was first tested on a series of well-defined and well-established polystyrene combs synthesized by Roovers et al. [2]. Table SI2 depicts the molecular characteristics of these combs. The developed model was used to predict the dynamic moduli in the frequency zone were branch relaxation dictates the overall rheological behavior, i.e. it is applied to moduli data from high frequencies down to the first relaxation step. This corresponds to frequency domain of 0.01 to 15000 rad/s for C732 and C742 and 0.1 to 15000 for C632 and C642 samples. The TMA parameters for polystyrene used in this work are adopted from Ref 3. The τ_e, G_N^0, and M_e^G are respectively fixed to 0.7ß10^{-3} s, 0.24 MPa, and 14 kg/mol. The Model predictions are compared with experimental data in Figure SI9 and the final results are listed in Table SI2.

Table SI2. Comparing experimental data with modeling results of sample comb structures.

	Experimental data			Modeling results			
Sample	$M_{backbone}$ (kg/mol)	M_{branch} (kg/mol)	N_{branch}	M_{branch} (kg/mol)	φ_{branch} (vol%)	N_{branch}	χ
C632	275	25.7	26	31.4	78	31	0.053

C642	275	47	29	41.5	85	38	0.033
C732	860	25.7	25	29.4	55	36	0.099
C742	860	47	29	42.0	71	50	0.071

As the fit to the second plateau and the following backbone relaxation was not the intension of the developed model, the corresponding frequency zones were not included in the optimization course. Despite using a constant set of material parameters, the overall agreement between model and experimental data is encouraging. The obtained branch lengths are also in very good agreement with the experimental data within less than 10% errors (see Table SI2). However the obtained volume fraction and the corresponding number of branches are less accurate. In other words the moduli domains where branches fluctuations are dominant are not significantly affected by the simultaneous relaxation of backbone free ends. This is not surprising as due to the high number of branches, the fractions of backbone free ends are insignificant. As we do not use this model to predict fraction and number of branches and instead, we use the conversion data of the second ATRP step for this purpose, it may not limit the application of the developed model for our purpose. The obtained conversion data can give the overall fraction of the branches and given the length of the branches obtained by this modeling approach, the number of branches can be predicted as well.

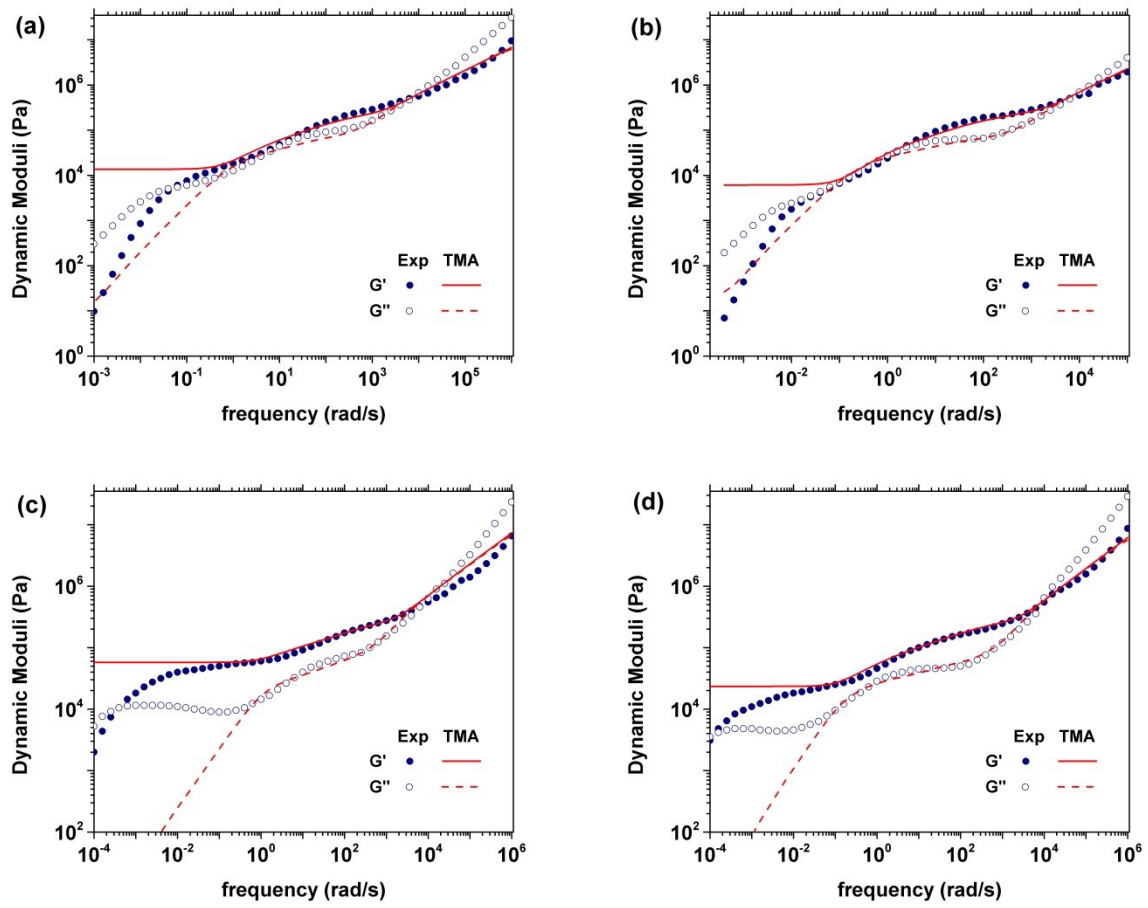

Figure SI9. Comparing model predictions with measured rheological properties for the sample polystyrene comb series (a) C632, (b) C642, (c) C732, and (d) C742.

5. References

[1] van Ruymbeke, E.; Keunings, R.; Bailly, C. J. Non-Newtonian Fluid Mech. 2005, 128, 7–22.

[2] Roovers, J.; Graessley, W. W. Macromolecules 1981, 14, 766–773.

[3] Ahmadi, M.; Keunings, R.; Bailly, C.; Nekoomanesh, M.; Arabi, H.; van Ruymbeke, E. Macromolecules 2011, 44, 647−659.